# Interface roughness and exchange bias - coercivity ratio in Pulsed-DC magnetron sputtered NiFe/IrMn/CoFe exchange bias trilayers

R. M. ÖKSÜZOĞLU*, O. DENIZ, M. YILDIRIM
*University of Anadolu, Faculty of Engineering, Department of Materials Sciences and Engineering, İki Eylül Campus, 26555 Eskişehir, Turkey*

$Ta/Ru/Ta/Ni_{81}Fe_{19}/Ir_{20}Mn_{80}/Co_{90}Fe_{10}$ exchange bias multilayer was grown by using pulsed DC unbalanced magnetron sputtering technique. The deposition pulse frequency of the NiFe seed layer has been varied between 10 – 50 kHz, by keeping all parameters of the remaining layers constant. The evolutions of the grain size, texture, interface roughness and the exchange bias ($H_{ex}$) and coercivity fields ($H_c$) including the $H_{ex}/H_c$ ratio have been systematically investigated. Grain size of the IrMn layer changes in the range of 8.9 nm–22 nm by constant layer thicknesses. The $H_{ex}$ is directly affected by the IrMn grain size for the bottom NiFe/IrMn interface, while it remains nearly insensitive to the grain size for the top IrMn/CoFe interface. The $H_{ex}$ at the NiFe/IrMn interface is largest if the grain size of the IrMn layer is same as the IrMn layer thickness. A direct relationship between the $H_c$ and grain size values was not observed; however, the $H_c$ is predominantly affected by the roughness of NiFe/IrMn and IrMn/CoFe interfaces. Results reveal that the texture and interface roughness plays an important role on the $H_{ex}/H_c$ ratio and deposition conditions for the ferromagnetic layer can be optimized using the variable deposition pulse frequency for a high $H_{ex}/H_c$ ratio in the investigated trilayer EB system.

(Received August 16, 2012; accepted April 11, 2013)

*Keywords*: Magnetic anisotropy; Magnetic properties of monolayers and thin films; Grain size; Interface roughness; Pulsed DC Magnetron Sputtering

## 1. Introduction

The exchange bias (EB) coupling between a ferromagnetic (F) layer and an antiferromagnetic (AF) pinning layer [1] was investigated intensively both experimentally and theoretically [2-6], due to its wide range applications for spin valve systems in spintronic devices. The underlying mechanisms of the EB field ($H_{ex}$) and the coercivity field ($H_c$) of the F layer are under intense investigations and depends on several factors: AF layer thickness, crystalline grain size, texture [4-16], role of the AF bulk moments [17, 18] or interfacial spin configuration [4, 5, 18-22], and interface/surface roughness in EB multilayer systems [8-10, 23-25].

Some of the effects of the AF grain size are expected to be similar to the AF thickness effects, $H_{ex}$ should decrease with reduced AF grain size. While the $H_{ex}$ reported to rise with the increasing grain size for some systems [26-28], for others the $H_{ex}$ decreases for larger grain sizes [29, 30]. In a recent study an increase of the $H_{ex}$ with increasing AF grain size was reported for low AF layer thicknesses (4-6 nm), however, a decrease of the $H_{ex}$ with AF layer thickness was also observed for thicker AF layers [5].

Regarding to the roughness, the $H_{ex}$ and $H_c$ seems to be relatively insensitive to the roughness value for several systems [8, 10, 23], while in others both parameters changes directly proportional to the roughness [25] or they indicate an opposite variation [24]. The relation between $H_{ex}$, $H_c$ and the roughness value was also reported to be dependent on the deposition conditions [9]. Other important factor is the $H_{ex}/H_c$ ratio, which is desired to be high for application [31], and influence of the microstructure on the $H_{ex}/H_c$ ratio is still one of the crucial points as it has not been investigated so far in EB trilayer systems. Thus, investigations on the effects of the grain size, texture and the interface roughness possess fundamental importance, since it will help to understand how these parameters can directly modify the EB parameters. For studies on EB systems, not only the deposition technique, but also the choice of the F and AF materials plays a key role. For most of the applications the IrMn/CoFe based EB system is the material of choice due to its high exchange anisotropy constant and high blocking temperature [12, 32].

In the present study, a pulsed DC unbalanced magnetron sputtering technique has been established in order to vary deposition conditions of the F layer by changing of the deposition pulse frequency at constant layer thickness, deposition power and pressure. The influence of the grain size, texture and interface roughness on the EB parameters, especially on the $H_{ex}/H_c$ ratio, in the NiFe/IrMn/CoFe EB trilayers have been systematically investigated.

## 2. Materials and methods

The Ta(5)/Ru(25)/Ta(5)/NiFe(6)/IrMn(10)/CoFe(2) /Ta(5) EB systems have been deposited by using pulsed DC unbalanced magnetron sputtering (Pulsed DC-MS) technique at room temperature (the numbers in parentheses are layer thicknesses in nanometres). A pulsed DC power source (Advanced Energy, Pinnacle Plus+ 5 kW) was used to control the current (~0.10 – 0.11 A) and the voltage (~350 V) supplied to the target materials (99.9% Kurt J. Lesker). The pulse was operated at a frequency of 50 kHz and had a width of 5 μs for all other layers except from the NiFe layer. During the deposition of the NiFe layer the pulse frequency was varied from 10 kHz to 50 kHz by a fixed width of 5 μs, in order to induce a grain size change through the NiFe/IrMn layers. The thickness of AF IrMn layer was chosen as 10 nm, since at this thickness the $H_{ex}$ for NiFe/IrMn and IrMn/CoFe based EB systems was reported to be the largest [7, 16]. Besides, it is believed that there is not any training effect at this AF IrMn thickness [33]. All EB samples were prepared onto Si/400 nm thermal $SiO_2$ substrates with an Ar gas pressure of 0.26 Pa and without substrate heating. The base pressure prior to the deposition was the order of $2.67 \times 10^{-7}$. An *in situ* in-plane external magnetic field of 0.5 kOe was applied during the growth, in order to saturate the soft ferromagnetic NiFe layer and induce unidirectional anisotropy at the NiFe/IrMn and IrMn/CoFe interfaces. The so-called unidirectional post-annealing was performed after deposition at 200°C for 1 hour under a vacuum better than $6.67 \times 10^{-5}$ Pa and then field-cooled to the room temperature in a magnetic field of 0.5 kOe along the same direction of the field applied during the deposition. Each set of specimens were grown in the same vacuum cycle.

X-Ray Diffraction (XRD) and specular X-Ray Reflectivity (XRR) measurements were carried out using a Bruker 4-circle diffractometer equipped with a Cu sealed tube point source and a Göbel Mirror optic to generate a 2D-collimated parallel beam (divergence ca. 0.03°, a lateral length of 18 mm). With a fixed slit assembly, the diffractometer system records specular XRR curves with a dynamic intensity range of roughly seven orders of magnitude. The experimental specular XRR data were analysed using the commercial Diffrac Plus LEPTOS software. Using a genetic algorithm, it obtains the best-fit simulation to the experimental data for multilayer structures by automatically adjusting the following parameters: the layer thicknesses $t_i$, root mean square roughness values $\sigma_i$ and mass densities $\rho_i$. To obtain adequate fits of the low-intensity data encountered in the high-θ region of the XRR curves, an absolute log weighting of the intensity difference between experimental and theoretical data was chosen for this work. Since the diffuse scattering contribution was negligible (~1.90 cps compared to measured incident intensity of $\sim 3 \times 10^7$ cps), it has not been subtracted from the measured specular reflectivity. No grading was found at interfaces in the investigated EB samples. Magnetization (*M-H*) loops were measured using a Physical Property Measurement System (PPMS – Quantum Design).

## 3. Results and discussion

### 3.1. Structure

XRD patterns of the EB samples with different pulse frequencies of the NiFe seed layer (see Fig.1) indicate the structures of the layers; fcc IrMn(111), fcc NiFe(111), hcp Ru(002) and bcc Ta(110). Additional information on the structure, i.e. grain size and texture of the EB samples were obtained by the peak profile fitting of XRD patterns using the commercial TOPAS software. The resulting values, the integral intensity and the full width at half maximum (FWHM) values are used to calculate the grains size and the crystal texture ratio. The average grain size of AF IrMn layer, calculated from the FWHM of the fcc IrMn(111) peak by using the Scherrer's equation, varies from 8.9 ± 0.25 to 22.1 ± 0.44 nm, whereas the grain size of the Ru layer remains almost constant (~ 21.7 ± 0.45 nm). In previous studies, it was also observed that grain size of the AF layer exceeds (in some deposition conditions) the thickness of the AF layer [5, 30]. The very broad low intensity diffraction peak of the NiFe layer does not allow calculating the grain size in the NiFe layer. These results reveal that the variation of the deposition pulse frequency in the NiFe layer induces a grain size change in the AF IrMn layer. Moreover, the crystal texture ratio (intensity/FWHM ratio of the selected XRD peak) was determined for the IrMn(111) diffraction peak and the highest crystal texture ratio was found for the lowest deposition pulse frequency giving the best <111> out-of-plane texture (Fig. 2). It means that the highest crystallographic texture was achieved at the largest grain size of the AF IrMn layer.

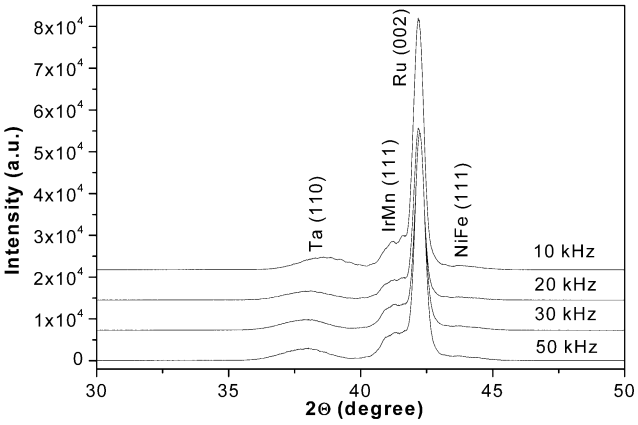


*Fig. 1 XRD patterns of the investigated EB samples for different pulse frequencies applied during the deposition of the NiFe seed layer.*

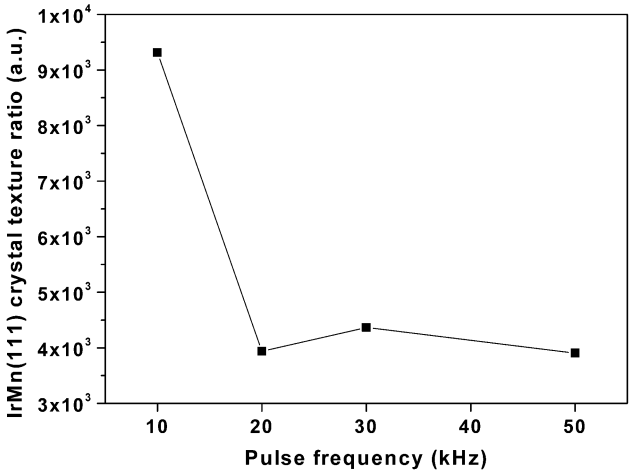


*Fig. 2 Crystal texture ratio of IrMn(111) for different pulse frequencies applied during the deposition of the NiFe seed layer.*

In the EB systems, it is generally not possible to keep the grain size constant, if the AF layer thickness is varied by keeping the deposition parameters fixed. With other words, grain size of the AF layer can be changed by the variation of the thickness [5] and the change of the AF layer thickness can induce variation of the texture and/or interface roughness [2]. If the grain size can be varied by a constant AF layer thickness, the influence of the grain size on the exchange bias parameters can be discussed more precisely. In order to find out the evolution of the individual functional film thicknesses and the interface roughness values upon the pulse frequency variation in the NiFe layer, a detailed XRR study was carried out. Fig. 3 shows the experimental XRR data of the samples and their corresponding best-fit curves. The individual thickness values obtained from best-fit simulations to the experimental data are illustrated in the Fig.4a,b. The thickness values of the Ru and IrMn layers together with the grain size of these layers were shown in Fig.4a, and the thickness values of the NiFe, Ta and CoFe layers in Fig.4b, both in dependence on the pulse frequency. The thickness values of all individual layers of the multilayer are consistent with the deposition values within the error factors and do not change with the deposition pulse frequency of the NiFe seed layer (Fig.4a,b). As shown in Fig.4a,b, only the grain size of the IrMn layer changes without any variation of the thickness of remaining layers. This proves that the grain size of the IrMn layer can be varied by the deposition pulse frequency of the NiFe seed layer without any thickness change of the functional layers in the investigated EB system.

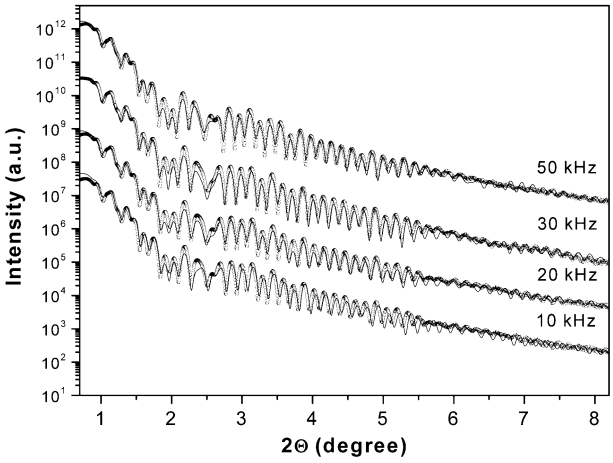


*Fig. 3. Experimental XRR data (open circles) and corresponding best fit simulations (straight lines) of the EB samples with different pulse frequencies applied during the deposition of the NiFe seed layer. The curves are vertically shifted for clarity.*

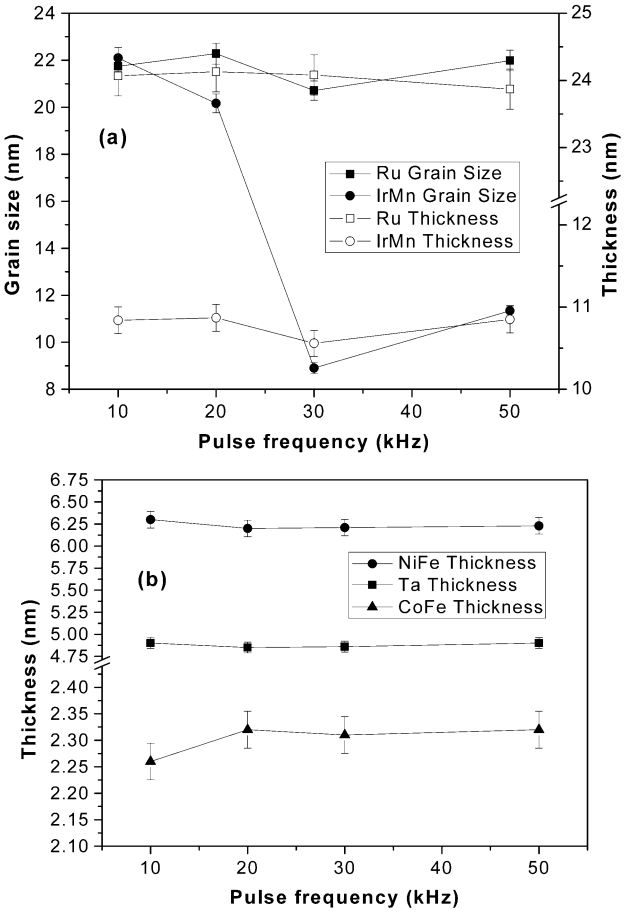


*Fig. 4 (a) Variation of the thicknesses and the grain size in the Ru and IrMn layers for different pulse frequencies applied during the deposition of the NiFe seed layer. (b) Evolution of the thicknesses of the NiFe, Ta and CoFe layers as a function of the pulse frequency. All lines are guide for the eye.*

Fig. 5 shows the interface roughness values at Ta/NiFe, NiFe/IrMn, IrMn/CoFe and CoFe/Ta interfaces, obtained from the best-fit of the XRR curves, as a function of the pulse frequency. The evolution of the interface roughness points out that the sequential deposition of the layers does not give rise to a cumulative interface roughness increase. The roughness values at the lower Ta/NiFe is higher than the upper CoFe/Ta interface and both values do not vary with the pulse frequency within the error factor (Fig.5). In contrast to that, the interface roughness values at NiFe/IrMn and IrMn/CoFe interfaces indicate a variation with pulse frequency (Fig.5), and the interface roughness at NiFe/IrMn were found to be larger than that of IrMn/CoFe interface (Fig.5). Considering of the evolution of the grain size and the interface roughness with the pulse frequency, a significant correlation could not be observed between the interface roughness values and the grain size of the IrMn layer.

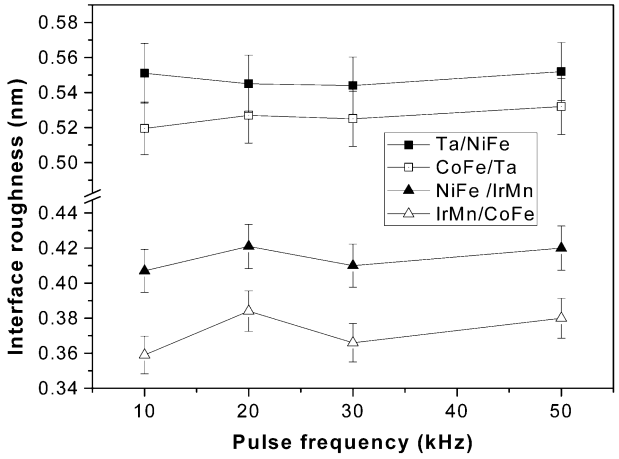


*Fig. 5 Evolution of the interface roughness values at the Ta/NiFe, NiFe/IrMn, IrMn/CoFe and CoFe/Ta interfaces, from the XRR best fit simulations (Fig.3), in dependence of the pulse frequency. All lines are guide for the eye.*

### 3.2. Magnetic properties

The *M–H* loops of the investigated EB systems were shown in Fig.6a-d. For all the EB samples with different pulse frequencies, two M–H loops are overlapped due to EB interactions between IrMn layer and magnetically hard CoFe pinned layer and between soft NiFe seed and IrMn layer (see Fig.6a-d). The resulting $H_{ex}$ values subtracted from *M–H* loops were called as $H_{ex}$-CoFe for the IrMn/CoFe and $H_{ex}$-NiFe for the NiFe/IrMn interface marked also in Fig.6a-d. In the inset pictures in Fig.6a-d, the exchange bias shifts at NiFe/IrMn interface were shown for better visualization. Fig.7 shows the $H_{ex}$-CoFe and $H_{ex}$-NiFe values as function of the pulse frequency. As can be seen in Fig.7, the $H_{ex}$-CoFe values do not vary significantly with the pulse frequency within the error factor, while the $H_{ex}$-NiFe increases with increasing deposition pulse frequency of the NiFe seed layer.

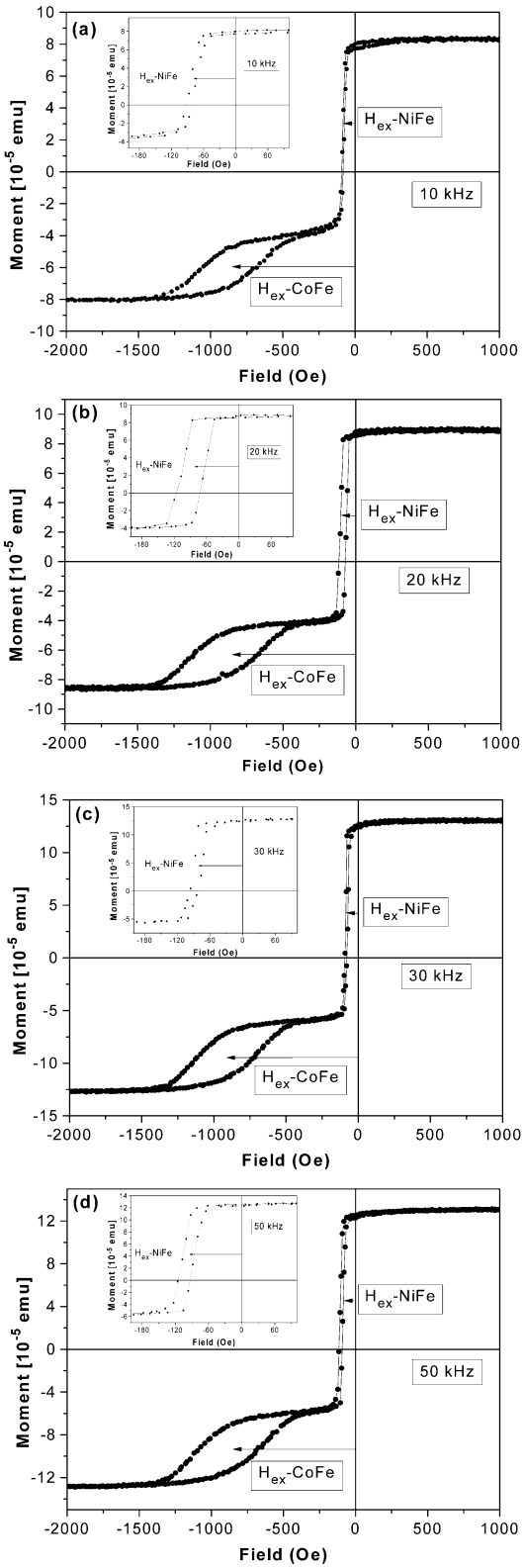


*Fig. 6 Magnetization (M-H) loops of all EB samples for different pulse frequencies; (a) 10 kHz, (b) 20 kHz, (c) 30 kHz and (d) 50 kHz. In all M-H loops, the EB fields at NiFe/IrMn and IrMn/CoFe interfaces were marked by arrows and called as $H_{ex}$-CoFe and $H_{ex}$-NiFe. All inlet pictures indicate the exchange bias shifts resulting at the NiFe/IrMn interface for better observation. All lines are guide for the eye.*

It seems that the exchange bias anisotropies at both interfaces do not affect each other through the 10 nm thick IrMn layer. In contrast to that, in a previous study on CoFe(4nm)/FeMn(10nm)/CoFe(4nm) trilayers prepared by ion beam deposition [18], an enhancement of the $H_{ex}$ at both bottom and top interfaces was reported. And this increase was attributed to propagation of the EB within the 10 nm AF FeMn layer [18]. According to authors, uncompensated (UC) spins are created favourably near the F/AF interface when an AF layer is deposited on a magnetized F layer. These interpretations were based on the following mechanism; deposition of a F layer on an AF layer in a magnetic field induce a competition between strong polarizing field produced by the surface magnetization of the F layer and the formation of the AF order in the AF layer. These result in a higher $H_{ex}$ at the bottom F/AF interface. The UC spins may also spread over the AF layer to the top AF/F interface, where creation of the UC spins less favored, leading to an improvement of the $H_{ex}$ at the top AF/F interface [18]. The enhancement of the $H_{ex}$ was also reported for the bottom NiFe/FeMn interface in the NiFe/FeMn/NiFe trilayers deposited by RF magnetron sputtering [17], and attributed to the growth of the FeMn layer on a magnetically saturated NiFe(111) layer. In the NiFe/IrMn/CoFe trilayer system investigated in the present study, an interaction between the NiFe and magnetic CoFe layers and/or any rise of the $H_{ex}$ at one of these interfaces cannot be directly deduced from *M–H* loops, namely due to the differences in the thickness and material of the NiFe and CoFe layers.

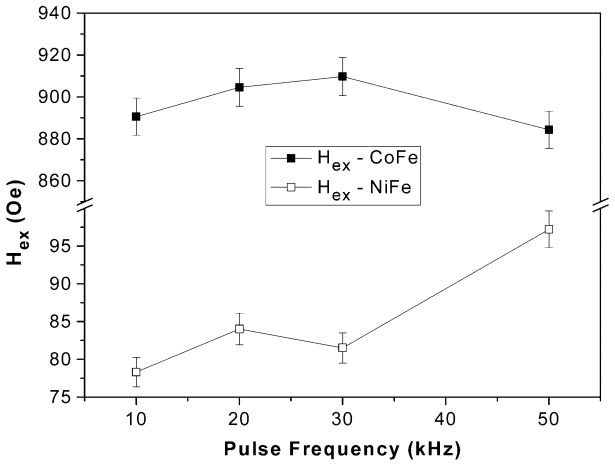


*Fig. 7 Changes of the $H_{ex}$-CoFe and $H_{ex}$-NiFe values calculated from M-H loops (Fig.6) in dependence of the pulse frequency. All lines are guide for the eye.*

Since in the investigated trilayers, the IrMn layer was grown on the NiFe(111) seed layer under *in-situ* in-plane magnetic field, the observed change of the $H_{ex}$ with AF grain size at the NiFe/IrMn interface by an almost constant $H_{ex}$ at IrMn/CoFe interface (see in Fig.7 and Fig.8), can be interpreted as follows: The pulse frequency variation during the deposition of the seed NiFe layer induces a grain size change in the <111> out-of plane oriented AF IrMn(111) layer. Hence, the interaction between the surface magnetization of NiFe layer and the formation of the AF order in the IrMn layer occurs through an interface area along the [111] direction. Thus, if most of the AF grains within the 10 nm thick IrMn layer are accepted as saturated, namely up to the top IrMn/CoFe interface, a remarkable variation of the $H_{ex}$ at IrMn/CoFe interface cannot be expected.

Another important point is the effect of the interface roughness. Both the evolution of the $H_{ex}$ (Fig.7) and the interface roughness values (Fig.5) do not give rise to a correlation between them. In addition to that, the interface roughness values, shown in Fig 5, are not directly affected by the grain size in the IrMn layer (Fig.4a). Hence, the variation of the $H_{ex}$ seems to be insensitive to the interface roughness at both bottom NiFe/IrMn and top IrMn/CoFe interfaces. Consequently, the variation of the $H_{ex}$-NiFe with deposition pulse frequency can clearly be related to the grain size change. In Fig.8, the $H_{ex}$-NiFe values were given as function of the grain size of the IrMn layer. The $H_{ex}$-NiFe first increases with rising grain size from ~8.9 nm up to ~11 nm and decreases with increasing grain size. The maximum of the $H_{ex}$-NiFe value is observed where the grain size value is same as the thickness of the IrMn layer, which reflects a clear coherence between the grains size and the thickness of the AF layer in the growth direction, resulting in highest exchange bias field. The $H_{ex}$-NiFe does not linearly correlate to the grain size, which explains also the drop of the $H_{ex}$-NiFe value in Fig.7 for the pulse frequency of 30 kHz, corresponding to the lowest grain size in IrMn layer. In our previous study, such a clear correlation between the AF grain size and $H_{ex}$-NiFe could not be observed, where the grains size change was induced by variation of the NiFe layer thickness [6]. According to the results in the present study, it can be understood that there are two different regimes in our samples where the grain size is almost equal to the layer thickness (high $H_{ex}$) and larger than the layer thickness (low $H_{ex}$).

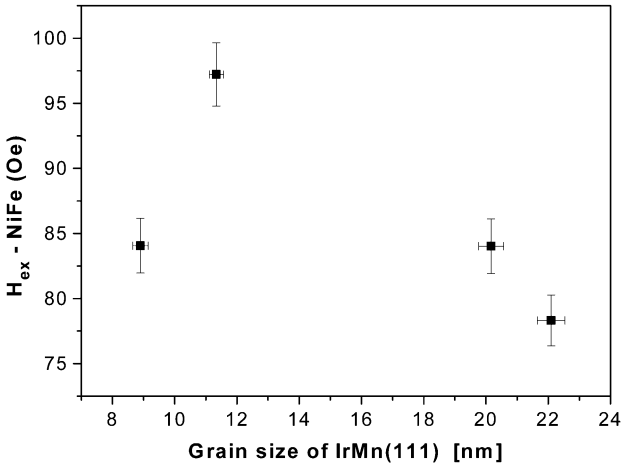


*Fig. 8 Evolution of the $H_{ex}$-NiFe values as function of the grain size of the IrMn layer calculated from FWHM of fcc IrMn(111) peak in the XRD pattern (Fig.1) by using the Scherrer equation.*

The other important EB parameter is the $H_c$. The results do not indicate a direct relationship between the grain size of the IrMn layer and the $H_c$ at both NiFe/IrMn and IrMn/CoFe interfaces. However, the evolutions of the $H_c$ and the interface roughness with pulse frequency (see Fig.9a,b) point out a relation between them. Both the $H_c$-NiFe and $H_c$-CoFe values (Fig.9b) indicate a maximum at the pulse frequency of 20 kHz and possess same variation with frequency change (Fig.9b). The evolutions of the interface roughness values at NiFe/IrMn/CoFe interfaces (Fig.9a) are same as that of the $H_c$ values (Fig.9b). The question, if the UC spins are creatable by the interface roughness induced by an interdiffusion at both interfaces, cannot be confirmed by the XRR technique, because it is not possible to distinguish between topological roughness and interdiffusion, both contributing to the interface roughness by this technique. The tendencies of both the $H_c$ and the interface roughness evidence clearly that the interface roughness play an important role on the coercivity in the NiFe/IrMn/CoFe EB trilayer system deposited by the Pulsed DC-MS technique.

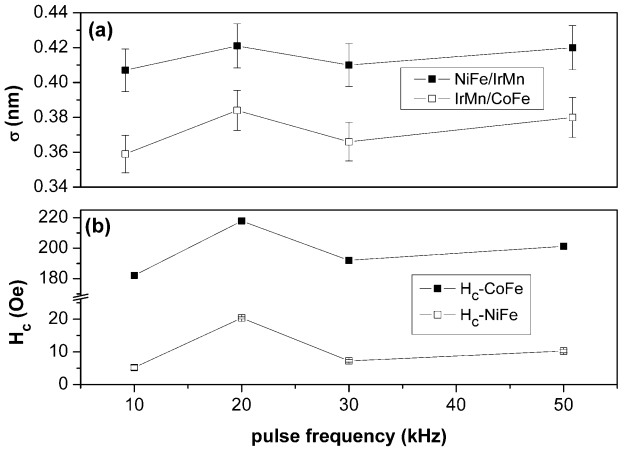


*Fig. 9 (a) Pulse frequency dependent evolution of the interface roughness values (σ) from the XRR best fit simulations (Fig.3), and (b) that of the $H_c$-NiFe and $H_c$-CoFe values from the M-H loops (Fig. 6) at NiFe/IrMn/CoFe interfaces. All lines are guide for the eye.*

In addition to the $H_{ex}$ and $H_c$ values, the $H_{ex}/H_c$ is also important to understand the magnetic interface quality of NiFe/IrMn/CoFe, since the $H_{ex}/H_c$ field should be increased for the sensor applications [31]. In Fig.10a,b, the change of the interface roughness values and $H_{ex}/H_c$ ratios for both NiFe/IrMn and IrMn/CoFe interfaces were given. The evolution of both the $H_{ex}/H_c$ ratio and interface roughness indicates an inverse relation between them. Thus, we may conclude that the interface roughness has a direct influence on the magnetic interface quality. As can be also seen in Fig. 10a,b, the highest $H_{ex}/H_c$ ratios (ca. 15 for NiFe/IrMn and ca. 4.9 for IrMn/CoFe interfaces) and the lowest interface roughness values were found for the EB sample deposited by the minimum pulse frequency of 10 kHz. The result for the IrMn/CoFe interface can be compared with the study of Fernandez-Outon et. al. [31], where they had achieved $H_{ex}/H_c$ ratio over 5. By considering of the crystal texture ratio given in Fig.2, it can be concluded that the highest crystal texture ratio together with lowest interface roughness favors the $H_{ex}/H_c$ ratio in the investigated EB trilayer system.

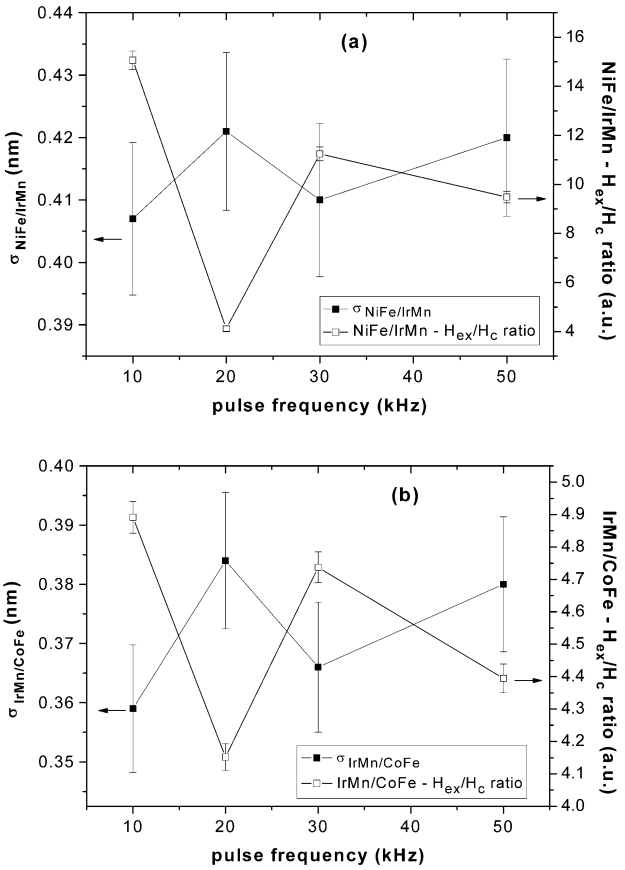


*Fig. 10 Pulse frequency dependent evolution of the interface roughness and $H_{ex}/H_c$ ratios (a) for the NiFe/IrMn and (b) IrMn/CoFe interfaces. All lines are guide for the eye.*

As a general result, the grain size dependence of the $H_{ex}$ reveals that the exchange bias is mainly dominated by volume effects induced by grain size. Other mechanisms, the texture and interface roughness plays a critical role on the evolution of the $H_{ex}/H_c$ ratio. Furthermore, the results indicate that the fabrication conditions of F layers in EB systems can be varied using the deposition pulse frequency for an optimization of the desired $H_{ex}/H_c$ ratio.

## 4. Conclusion

$Ta/Ru/Ta/Ni_{81}Fe_{19}/Ir_{20}Mn_{80}/Co_{90}Fe_{10}/Ta$ exchange bias systems have been grown by different pulse frequency in the range of 10 kHz to 50 kHz by using pulsed DC unbalanced magnetron sputtering technique. The evolution of the texture, grain size, interface roughness and their influence on the exchange bias parameters have been systematically investigated in dependence on the

deposition pulse frequency. The results underline the importance of the IrMn grain size for the exchange bias and the effect of the texture and interface roughness on the $H_{ex}/H_c$ ratio. The exchange bias is unaffected by the interface roughness. No correlation between the grain size and the interface roughness was observed. The results indicate clearly that the exchange bias field is highest, if the grain size of the IrMn layer is same as the IrMn layer thickness, indicating a significant coherence between the thickness and the grain size of the IrMn layer. A direct relationship between the coercivity values and the IrMn grain size was not observed; however, the coercivity values are predominantly affected by the interface roughness at both NiFe/IrMn and IrMn/CoFe interfaces. Largest IrMn grain size, highest texture and lowest interface roughness favour the $H_{ex}/H_c$ ratio. This reveals that the fabrication conditions of the ferromagnetic layer are important factor for the optimization of the $H_{ex}/H_c$ ratio at both interfaces in the trilayer EB system.

**Acknowledgements**

This work was partially supported by TUBITAK under Grant No MAG-106M517 and the Directorate for Scientific Research Projects of Anadolu University under Grant No BAP-050255 and BAP-1103F043.

## References

[1] W.H. Meiklejohn, C.P. Bean, Phys. Rev. **102**, 1413 (1956).
[2] J. Nogues, K. Ivan Schuller, J. Magn. Magn. Mater. **192**, 203 (1999).
[3] Susumu Soeya, Appl. Phys. Lett. 94, 242507 (2009).
[4] S.K. Mishra, F. Radu, S. Valencia, D. Schmitz, E. Schierle, H.A. Dürr, and W. Eberhardt, Phys. Rev. B **81**, 212404 (2010).
[5] K. O'Grady, L.E. Fernandez-Outon, G. Vallejo-Fernandez, J. Magn. Magn Mater. **322**, 883 (2010).
[6] Ramis Mustafa Öksüzoğlu, Mustafa Yıldırım, Hakan Çınar, Erwin Hildebrandt, Lambert Alff, J. Magn. Magn. Mater. **323**, 1827 (2011).
[7] Yuan-Tsung Chen, Nanoscale Res. Lett. **4**, 90 (2009).
[8] M. Pakala, Y. Huai, G. Anderson, L. Miloslavsky, J. Appl. Phys. **87**, 6653 (2000).
[9] Congxiao Liu, Chengtao Yu, Huaming Jiang, Liyong Shen, Alexander C, and G.J. Mankey, J. Appl. Phys. **87**, 6644 (2000).
[10] Luc Thomas, Béatrice Negulescu, Yves Dumont, Michel Tessier, Niels Keller, André Wack, Marcel Guyot, J. Appl. Phys. **93**, 6838 (2003).
[11] N. P. Aley, G. Vallejo-Fernandez, R. Kroeger, B. Lafferty, J. Agnew, Y. Lu, and K. O'Grady, IEEE Trans. Magn. **44**, 2820 (2008).
[12] Masakiyo Tsunoda, Ken-ichi Imakita, Mamiko Naka, Migaku Takahashi, J. Magn. Magn. Mater. **304**, 55 (2006).
[13] Kojiro Yagami, Masakiyo Tsunoda, Migaku Takahashi, J. Appl. Phys. **89**, 6609 (2001).
[14] J. Van Driel, F.R. de Boer, K.M.H. Lenssen, R. Coehoorn, J. Appl. Phys. **88**, 975 (2000).
[15] Yiming Mahendra Pakala, Huai, Geoff Anderson, IEEE Trans. Magn. **36**, 2620 (2000).
[16] Ken-ichi Imakit, Masakiyo Tsunoda, Migaku Takahashi, J. Appl. Phys. **97**, 10K106 (2005).
[17] V. K. Sankaranarayanan, S. M. Yoon, D. Y. Kim, C. O. Kim, C. G. Kim, J. Appl. Phys. **96**, 7428 (2004).
[18] D.N.H. Nam, W. Chen, K.G. West, D.M. Kirkwood, J. Lu, S.A. Wolf, Appl. Phys. Lett. **93**, 152504 (2008).
[19] R. Morales, Li. Zhi-Pan, J. Olamit, Kai Liu, J.M. Alameda, and K. Ivan Schuller, Phys. Rev. Lett. **102**, 097201 (2009).
[20] J-S. Lee, C-C. Kao, H. Jang, K-T. Ko, J-H. Park, K. Rhie, J-Y. Kim, J. Phys. Condens. Matter. **23**, 256001 (2011).
[21] Naoki Awaji, Toyoo Miyajima, Shuuichi Doi Kenji Nomura, J. Phys. Condens. Matter. **22**, 474012 (2010).
[22] G. Vallejo-Fernandez, M. Vopsaroiu, L.E. Fernandez-Outon, K. O'Grady, IEEE Trans. Magn. **42**, 3008 (2006).
[23] A.M. Zhang, H.L. Cai, X.S. Wu, J. Supercond. Nov. Magn. **23**, 863 (2010).
[24] V.P. Nascimento, E.C. Passamani, A.D. Alvarenga, F. Pelegrini, A. Biondo and E. Baggio Saitovitch, J. Magn. Magn. Mater. **320**, e272 (2008).
[25] C. Fleischmann, F. Almeida, J. Demeter, K. Paredis, A. Teichert, R. Steitz, S. Brems, B. Opperdoes, C. Van Haesendonck, A. Vantomme, K. Temst, J. Appl. Phys. **107**, 113907 (2010).
[26] M. Tsunoda, Y. Tsuchiya, M. Konoto, M. Takahashi, J. Magn. Magn. Mater. **171**, 29 (1997).
[27] M. Tsunoda, M. Konoto, K. Uneyama, M. Takahashi, IEEE Trans. Magn. **33**, 3688 (1997).
[28] Ryoichi Nakatani, Hiroyuki Hoshiya, Katsumi Hoshino, Yutaka Sugita, J. Magn. Magn. Mater. **173**, 321 (1997).
[29] Hiroko Uyama, Yoshichika Otani, Kazuaki Fukamichi, Osamu Kitakami, Yutaka Shimada, and Jun-ichi Echigoya, Appl. Phys. Lett. **71**, 1258 (1997).
[30] Kentaro Takano, R. H. Kodama, A. E. Berkowitz, Phys. Rev. Lett. **79**, 1130 (1997).
[31] L. E. Fernandez-Outon, K. O'Grady, S. Oh, M. Zhou M. Pakala, IEEE Trans. Magn. **44**, 2824 (2008).
[32] Ken-ichi Imakita, Masakiyo Tsunoda, Migaku Takahashi, Appl. Phys. Lett. **85**, 3812 (2004).
[33] A. Kohn, J. Dean, A. Kovacs, A. Zeitser, M. J. Carey, D. Geiger, G. Hrkac, T. Schrefl, and D. Allwood, J. Appl. Phys. **109**, 083924 (2011).

*Corresponding author: rmoksuzoglu@anadolu.edu.tr